



Quantifying terminal white bands in *Salix* from the Yenisei river, Siberia and their relationship to late-season flooding

Richard D. Thaxton^{1,2}  · Irina P. Panyushkina¹ · David M. Meko¹ · Georg von Arx^{3,4} · Leonid I. Agafonov⁵

Received: 11 August 2022 / Accepted: 3 January 2023

© The Author(s) 2023

Abstract

Key Message Wood fiber cell wall thickness best characterizes white bands found at the end of certain growth rings in *Salix alba*. Evidence suggests these features are related to late-season hydrology.

Abstract Recent, record-breaking discharge in the Yenisei River, Siberia, is part of a larger trend of increasing river flow in the Arctic driven by Arctic Amplification. These changes in magnitude and timing of discharge can lead to increased risk of extreme flood events, with implications for infrastructure, ecosystems, and climate. To better understand the effect of these changes on riparian tree growth along the lower reaches of the Yenisei River, we collected white willow (*Salix alba*) cross sections from a fluvial fill flat terrace that occasionally floods when water levels are extremely high. These samples displayed bands of lighter colored wood at the end of certain annual growth rings that we hypothesized were related to flood events. To identify the characteristics and causes of these features, we use an approach known as quantitative wood anatomy (QWA) to measure variation in fiber cell dimensions across tree rings, particularly fiber lumen area (LA) and cell wall thickness (CWT). We investigate (1) which cell parameters and method to extract intra-annual data from annual tree rings best capture terminal white bands identified in *Salix*, and (2) if these patterns are related to flood magnitude and/or duration. We find that fiber CWT best captures terminal white bands found in *Salix* rings. Time series derived from CWT measurements correlate with July water-level durations, but at levels too low to be labeled flooding. Although both terminal white bands and July flooding have reduced since 1980, questions remain as to the cause of terminal white bands. Understanding how riparian vegetation responds to changes in hydrology can help us better manage riparian ecosystems and understand the impacts of a changing Arctic hydrological regime.

Keywords Quantitative wood anatomy · Wood fibers · Intra-annual density fluctuation · Yenisei River Basin · Hydrology · Riparian vegetation

Introduction

Communicated by Sergio Rossi .

✉ Richard D. Thaxton
rthaxton@arizona.edu

¹ Laboratory of Tree-Ring Research, University of Arizona, Tucson, AZ, USA

² School of Natural Resources and the Environment, University of Arizona, Tucson, AZ, USA

³ Swiss Federal Institute for Forest, Snow and Landscape Research WSL, Birmensdorf, Switzerland

⁴ Oeschger Centre for Climate Change Research, University of Bern, Bern, Switzerland

⁵ Institute of Plant and Animal Ecology UB RAS, 202 Marta 8th St., Yekaterinburg 620144, Russia

River discharge in the pan-Arctic has intensified over the last century and will likely continue to change in coming decades (IPCC 2021). Hydrological changes are driven by Arctic Amplification—a positive feedback loop of accelerating warming over the Arctic resulting in a combination of increasing surface air temperature, melting of sea ice and permafrost, and increased precipitation in northern latitudes (Screen and Simmonds 2010; Shiklomanov et al. 2013). This forcing is able to produce record-setting river discharge that is part of an accelerating trend (Shiklomanov and Lammers 2009). Although hydrological changes across and within river basins are heterogenous, the net effect is an increase in freshwater export to the Arctic Ocean in spring, summer and even winter (Panyushkina et al. 2021; Feng et al. 2021).

There are strong expectations for these trends to continue during the rest of the twenty-first century (Carmack et al. 2016; Bring et al. 2017; Zanowski et al. 2021). On the global scale, these changes may have critical implications for ocean circulation (Serreze and Francis 2006; Jones et al. 2008; Weijer et al. 2020, but see He and Clark 2022), global climate (Coumou et al. 2018), and human trade and navigation (Smith and Stephenson 2013). On the ecosystem and plant scale, increased flooding will potentially alter Arctic ecosystem function and impact plant physiology (Fan et al. 2020).

Tree rings can be instrumental for providing long-term context to more frequent floods and altered hydrology (Meko et al. 2012; Ballesteros-Cánovas et al. 2015). Existing instrumental discharge records in the Arctic are often sparsely located and short, creating a need for additional data (Bring et al. 2017). Tree-ring records derived from conifers have been used to successfully extend discharge records across the pan-Arctic by hundreds of years (MacDonald et al. 2007; Agafonov et al. 2016). These studies provide critical insight not only into long-term annual discharge trends, but into seasonal trends as well (Panyushkina et al. 2021). Dendrochronology of angiosperms offers an opportunity to fill even more of these gaps, particularly when it comes to capturing extreme hydrological events. Angiosperm wood anatomical response to flooding is dependent on both the timing and magnitude of the discharge. The largest floods tend to have a direct effect on vegetation via impact and scarring, with floods recorded as reduced xylem vessel lumen area or increased fiber lumen area in the injured ring (Ballesteros et al. 2010; Arbellay et al. 2012). Even if the tree is not physically injured, flood events can still be recorded in tree rings. Most research into angiosperm anatomical response to non-injurious flooding relies on vessel measurements from ring-porous species (trees with conspicuously larger vessels in the earlywood than latewood) (Ballesteros-Cánovas et al. 2015). Anomalous rings formed during peak spring discharge tend to produce earlywood vessels of reduced size which can be identified visually and can help understand flood history (Meko and Therrell 2020; Nolin et al. 2021). Even small changes in vessel size are physiologically important since theoretical hydraulic conductivity scales with vessel diameter to the power of four, as illustrated by the Hagen-Poiseuille law (Tyree and Ewers 1991). Chronologies of vessel area and vessel number are particularly useful for capturing large spring discharge because, unlike ring width, the relationship is maintained even for very large discharges (Kames et al. 2016). The caveat is that only a short window (2–3 weeks) exists for the tree to record this information, limiting its utility (Kames et al. 2016).

When researchers have used diffuse-porous angiosperms (no clear separation of earlywood and latewood) to study flood history, they typically rely on vessel characteristics. Diffuse-porous species response to flooding appears to

vary by species and biome. For example, recent work with *Alnus glutinosa* showed no relationship between prolonged flood events and vessel characteristics (Anadon-Rosell et al. 2022). In contrast, Lopez et al. (2014) examined the tropical species *Prioria copaifera* and found chronologies of vessel number could be used to reconstruct flood height, as most radial growth occurred during flood years (López et al. 2014). Other studies have even related vessel distribution (i.e., tangential vessel bands) to prolonged flood inundation (Tardif et al. 2021).

While the utility of vessel elements appears well established, there is a need to understand the utility of other wood cellular components such as wood fibers. Fibers provide mechanical strength to the wood, and, although little or not involved in the actual xylem transport of water, may contribute to healthy vessel function through cavitation resistance (Carlquist 2001; Hacke et al. 2000; Schoch et al. 2004; De Micco et al. 2016a, b). Exploration of fibers is still in its infancy, but interest is growing (Janssen et al. 2020). Research into the flood response of riparian *Salix* trees along the Ob River, Siberia, revealed extreme flood events were captured as extremely narrow rings or rings with sudden changes in wood fibers (Meko et al. 2020). Wood fibers have also been reported to be as sensitive to environmental fluctuations as vessel chronologies, confirming their utility (De Micco et al. 2016a, b). However, they may not be useful for every research question, as wood fiber measurements of flooded alder showed no relationship between extreme flooding and cell wall thickness (CWT) (Anadon-Rosell et al. 2022). Still, some research does suggest wood fibers have the capacity to record flood events, at least for ring-porous species. The most relevant study is work by Yanosky (1984), which related increased wood fiber size and decreased cell wall thickness near the end of the annual growth ring to flooding events late in the growing season. This study, which examined riparian ash (*Fraxinus*) near Washington, D.C., USA, found white bands appeared more frequently in flood years and hypothesized that these fluctuations were essentially ‘growth spurts’ in which flooding of the root zone allowed drought-stressed trees to take advantage of additional water. Fluctuations tended to occur most often when the tree was younger and appeared on the wood surface as a white terminal band forming before the earlywood of the following year (Yanosky 1984).

We identified rings similar to those described by Yanosky in wood samples of diffuse-porous *Salix alba* (white willow) sampled in the summer of 2020 along the Yenisei River, Siberia. As with Yanosky, *Salix* tree cores contained bands of whiter wood visible from the sanded core surface. These white bands appeared in both the early and late portions of tree rings, but were more frequent at the end of annual growth rings. For this reason, we chose to focus on white bands at the end of growth rings, referred to here as terminal

white bands. Upon further examination of *Salix* rings using anatomical thin sections, we determined terminal white bands corresponded to larger wood fibers (Fig. 1). These changes occurred in wood fibers only and were unaccompanied by an equivalent change in vessel size or density.

Given these anomalies' potential relationship to late-season flooding, they may prove useful for understanding flood variability in this globally important watershed. Additionally, since these white bands represent changes in fiber characteristics, investigation into these wood anomalies offers a chance to provide much-needed research into quantifying physical characteristics of wood fibers in diffuse-porous species. Recent advances in the field of quantitative wood anatomy (QWA) offer an opportunity to measure characteristics of these terminal white bands at the level of individual cells, building time series to compare with hydrologic data. Understanding intra-annual variation in tree rings allows us to probe into subtle, intra-annual changes in the basin's hydrology.

For these reasons, the following research explores both the characteristics of *Salix* terminal white bands and their relationship to flooding. First, we identify which QWA measurement (cell wall thickness (CWT) or lumen area (LA)) and which measurement averaging method allows us to best quantify terminal white bands. We test two measurement averaging methods in this study: (i) CWT or LA was averaged over a fixed width (50–150 μm) from the ring

boundary, and (ii) CWT or LA was averaged over a percentage of the ring (>87.5–95%) closest to the ring boundary, an approach referred to as sectoring. Second, we investigate how white bands relate to flood magnitude and duration. We hypothesize that fiber cell wall thickness would better capture these features than fiber lumen area, which would be further improved when cell wall thickness of each cell is normalized by the average cell wall thickness of the ring. Additionally, we expected that averaging cells based on their measured position in the ring would better quantify white bands than using the relative position. We hypothesize the best combination of cell measurements and methods would illuminate a relationship between terminal white bands and flood events late in the growing season. Understanding how best to measure these unique features can help us better attribute their cause and may improve our understanding of short-lived intra-annual hydrologic events throughout the lower Yenisei River basin and their effect on vegetation.

Materials and methods

Characterization of study site and river discharge

The study site (Fig. 2) is located on an island at the confluence of the Turukhan and Yenisei Rivers, roughly 10 km downstream from the city of Turukhansk (Krasnoyarsk Krai; 65.86 N, 87.74 E). The climate of this area is classified as continental sub-arctic, with mild summers and extremely cold winters (Beck et al. 2018). Climatological and hydrological information is summarized in Supplemental Figure 1. A riparian forest dominated by *Salix alba* (white willow) exists at the top of this terraced island, roughly 12–15 m above the median water level, excluding the June–July flood period (3.6 m asl). In general, the growing season for these trees lasts from mid-May to early September and the forest forms an open canopy with a dense understory of herbaceous plants and tall grasses. The elevation of the top of the island does not vary more than a meter over the study site.

In August 2020, we collected stem cross sections from 7 willow trees using a chainsaw, targeting dominant trees that appeared noticeably older. Trees were sampled in close proximity to each other, no more than 10–20 m apart. Wood disks were cut between 0.7 and 0.8 m above the ground. The wooden disks were transported to the Laboratory of Tree-Ring Research in Tucson, Arizona, for sample preparation, ring-width measuring, and chronology development following standard practices in dendrochronology (see Supplemental Text 1 for more detail). We used the program SEASCORR (Meko et al. 2011) to investigate the relationship between tree growth and discharge (Yenisei at Igarka, station code 9803, 67.43 N, 86.48 E), mean monthly temperature and total monthly

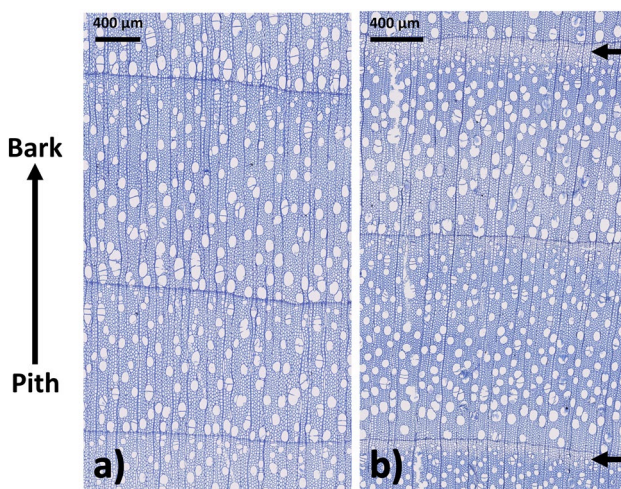


Fig. 1 Comparison of rings with and without terminal white bands. White bands are a type of intra-annual density fluctuation (IADF) or regions where abrupt changes in density occur (De Micco et al. 2016a, b). Rings are progressively older from the bottom to top of the image. **a** Rings 2017–2020 from tree BSH01. These years do not show a terminal white band, as there is little variation in wood fibers over the width of the ring. **b** Rings 1955–1958 from tree BSH03. Years 1955 and 1957 show distinct terminal white bands (black arrows) **b** Rings 1955–1958 from tree BSH03. Years 1955 and 1957 show distinct terminal white bands (black arrows) (Colour figure online)

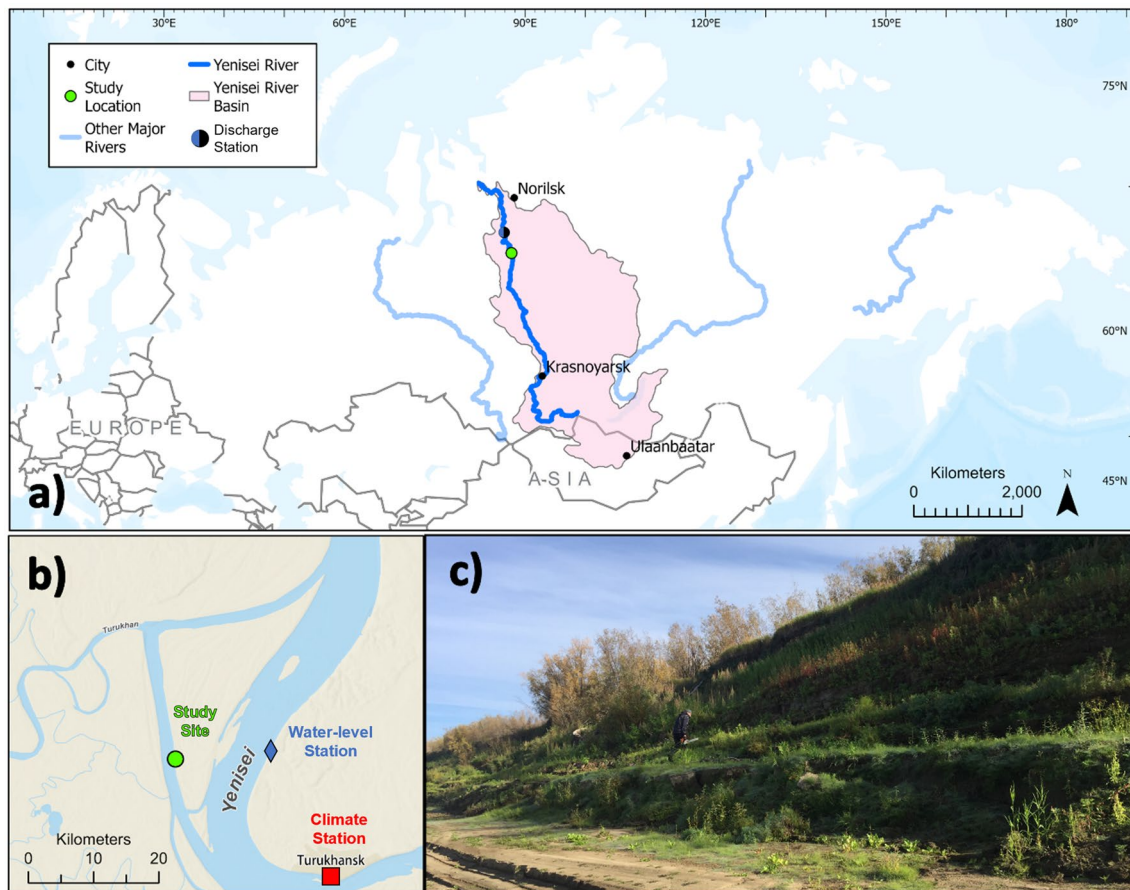


Fig. 2 Illustration of the study site. Panel **a** shows the geographic location of the Yenisei River basin (pink polygon) and Yenisei River (dark blue line) in relation to other major Arctic rivers (light blue). The study location is shown as a green dot. The discharge station (Yenisei at Igarka, station code 9803; blue and black circle) is located roughly 185 km downstream of the study site. **b** Location of the study site in relation to island at the confluence of the Turukhan and Yenisei Rivers. The study site is roughly 10 km downstream from the town of Turukhansk. Nearby gages provide water-level data (Selevan-

ikha, gauge code 9801; blue diamond) and climate data (Turukhansk, WMO Code 23,472; red square). **c** Vertical profile of island. The riparian forest sampled rests at the top of a terraced island, roughly 12–15 m above the average annual water surface (3.6 m asl). The median annual maximum water level is 17.5 m above the water's surface, but can reach up to 22 m during peak flows. Elevations estimated using the online tool ArcticDEM (Porter et al. 2018) (Colour figure online)

precipitation (Turukhansk, WMO Code 23,472, *GHCN-M v3.3.0.20190817*, 65.78 N, 87.93 E, elevation: 64 m asl; see Supplemental Fig. 1 for additional site information) (Menne et al. 2018).

We examined climatic relationships both including and excluding the period 1980–1993 when the flow regime was altered due to extensive damming on the Yenisei River. Discharge of the Yenisei River is driven by snowmelt with peak flows typically occurring in early June (Supplemental Figure 1c). Water-level data were obtained from the Selevanikha gauge (code 9801; 65.86 N, 87.87 E; Supplemental Figure 2). While July flows pale in comparison to the massive discharge in June, important changes in water level and flood duration are still evident (Fig. 3). July flows have decreased to the point July water levels

have not reached 10 m since 1992, despite this being a frequent occurrence prior.

Characterization of white bands, anatomical sample preparation and quantitative wood anatomical analysis

In addition to developing a ring-width chronology, we characterized terminal white bands as they appeared on thin sections. First, we developed a character list identifying years with white bands and classified anatomical anomalies based on their occurrence in the 'early' or 'late' portion of the growth ring (Yamaguchi 2011; De Micco et al. 2016a, b). The total number of trees showing terminal white bands were then tallied for each year to build a frequency histogram. After identifying all bands, we investigated if they

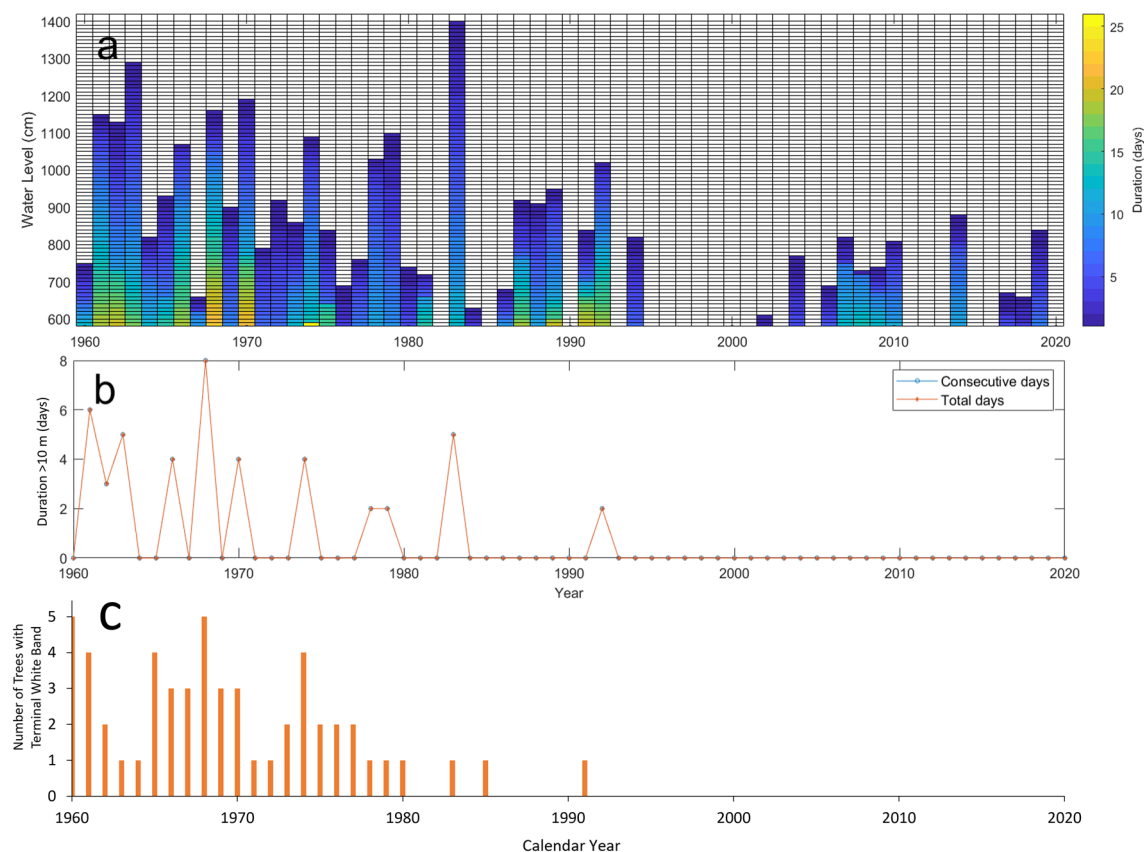


Fig. 3 July daily water levels and durations at Selevanikha (gauge code 9801), 1960–2020. The zero water level for this gage is 1.26 m above sea level. Gauge location is just downstream of the study site and 6 km east. **a** Number of days water levels reached a particular value. July water levels do not exceed 14 m and water levels above

7 m do not typically last longer than 15 days. **b** Time series of total days and consecutive days water level fell at or above 10 m. No data available for years 1993, 1995–98, and 2000–01. **c** Frequency histogram with the number of trees that contained a terminal white band (orange bars) in a particular year (Colour figure online)

were related to ring age or ring width. For ring age, we plotted white-band frequency as a function of tree age. For ring width, we measured the width of each visually identified white band in Image-Pro Plus (v6.1; Media Cybernetics) on thin section images and used Pearson correlations to investigate the relationship between terminal white-band width and ring width.

All samples were prepared for quantitative wood anatomy using procedures similar to other research (Edwards et al. 2020; Anadon-Rosell et al. 2022). 12 μm thin sections were cut from pieces of each slab using a rotary microtome (Thermo Scientific Microm HM 355S Microtome, Waltham, MA). Thin sections were stained with cresyl violet acetate (0.5 g per 250 ml H_2O), rinsed with solutions of increasing ethanol concentration (50%, 100%), and permanently affixed to slides using Eukitt mounting medium. Slide imaging was performed at the Swiss Federal Institute for Forest, Snow and Landscape Research WSL (Birmensdorf, Zürich, Switzerland) using a Zeiss Axio Scan Z1 (Carl Zeiss AG, Germany). From each

tree, thin section images from at least 1965–1980 were selected for further analysis because the majority of terminal white bands occurred in this time frame. Automatic detection of wood fibers from images was performed using ROXAS (von Arx and Carrer 2014). Although the program is typically used with conifers, it is also effective for identifying anatomical features in diffuse-porous species (von Arx et al. 2013; Wegner et al. 2013; Anadon-Rosell et al. 2022). We observed fibers in our samples to have a lumen area $< 500 \mu\text{m}^2$, and therefore, all larger cells were automatically removed. For each image, we then performed manual correction of the ROXAS-identified cells. Any improperly identified cells (e.g., fiber cell identified as vessel or ray parenchyma) or cells with collapsed cell walls were deleted. All ring borders were drawn manually since cell size transitions were subtle (Wegner et al. 2013) and ROXAS-derived ring-width measurements were compared to manually measured ring widths to ensure each ring was assigned to the proper calendar year. Upon completion of manual user correction, output Excel documents for each image and cell type were created with multiple measured

parameters. For subsequent analysis, only fiber LA and CWT were considered.

Data processing and statistical analysis

To determine how to best quantify the terminal white bands in our samples, we compared two approaches of averaging cell parameters (Fig. 4). Each approach used R scripts modified from the SECTOR.R code developed by Richard Peters (<https://deep-tools.netlify.app/2020/11/24/sector-intro/>), the angiosperm-equivalent of the RAPTOR R package used to prepare and visualize anatomical data from conifer tracheids (Peters et al. 2018).

The first approach averaged cell measurements over an area proportional to the total ring width, referred to as sectoring (Edwards et al. 2020; Gebregeorgis et al. 2021) (Fig. 4b). Rings were divided into $n=8$, 10, or 20 equal-sized sectors and we developed time series of average cell measurements in the n th sector. This corresponds to averaging cell measurements over 87.5–100%, 90–100%, and 95–100% of the ring. Unlike fixed-widths, sectoring helps account for the timing of ring formation by allowing the averaged band to vary with ring width.

In the second approach, we averaged each cell parameter within 50, 100, and 150 μm from the ring boundary

(Fig. 4c). These values were based on the mean white-band width (157.7 μm , $\sigma=8.9 \mu\text{m}$, $n=131$) and the minimum width (50 μm) for all trees. We applied this method to rings with and without terminal white bands to create a continuous time series of cell measurements. In this case, averaged bands of cell measurements are independent of ring width. The approach derives averaged bands directly from measured characteristics of white bands, allowing us to specifically target these anomalies.

For each method above, we determined if normalizing cell parameters could further improve quantification of white bands. Prior to averaging all cell measurements (CWT, LA) within a sector, cell parameters were normalized by dividing each cell measurement by the average cell measurement from the non-white portion of the ring only. For each combination of cell parameter averaging method and normalization, we then used a Welch test (Gans 1981) to identify which combination of methods could most strongly differentiate between rings with and without terminal white bands. We expected that normalization could better distinguish between rings with and without terminal white bands.

To assess which averaging method best agreed with our visual identification of terminal white bands, we used point-biserial correlation to estimate the relationship between the presence of terminal white bands and measured cell parameters (Bedrick 2005). Point-biserial correlation is an estimate of the product-moment correlation (r_b) in the case where one variable is dichotomous (i.e., white band presence/absence) and the other is continuous (i.e., CWT/LA). Correlation values obtained from this method, like Pearson's product-moment correlation (r), indicate the strength of the relationship between two variables. The point-biserial correlation was performed in R (Rizopoulos 2007; v. 3.6.3; R Core Team 2020) after confirming the data met assumptions of normal distributions (Shapiro and Wilk 1965; Royston 1995), and equal variances (Brown and Forsythe 1974; Gastwirth et al. 2009).

Using the best combination of cell measurements and cell averaging method above, we built mean cell chronologies. We calculated the mean cell parameter for each year from all trees to create the chronology and compared it to the number of days in July the water level exceeded a particular height. Long-term trends were present in both our cell and water-level duration time series which can inflate correlation values. To address this, we first-differenced each series to remove the long-term trends that would influence the relationship strength. We then calculated the Pearson correlation coefficient (r) between the mean chronology and water-level durations. To account for the effect of autocorrelation on the correlation significance, we used the adjusted degrees of freedom when calculating our p values (Dawdy and Matalas 1964; Hu et al. 2017). All correlations were limited to the

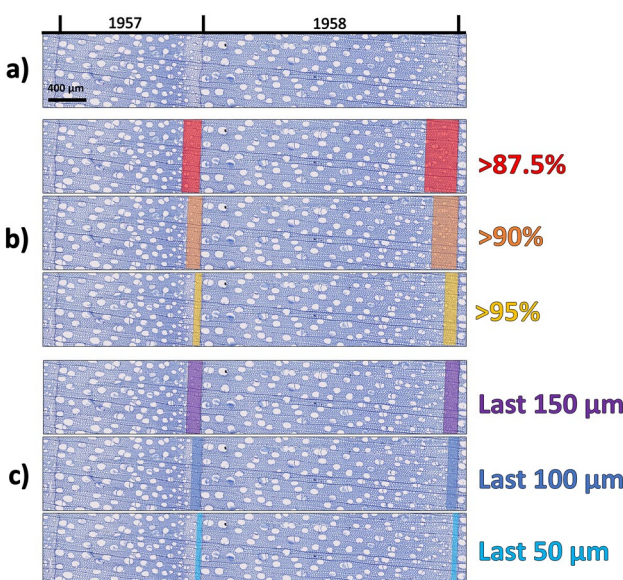


Fig. 4 Two approaches to averaging cell parameters. **a** Thin section depicting years 1957 and 1958. **b** Sectoring approach. CWT/LA for each ring were averaged over 87.5–100% (red), 90–100% (orange), and 95–100% (yellow) of the ring. Note that the area of averaged cell parameters increases as ring width increases. **c** Fixed-width approach. CWT/LA for each ring were averaged over the last 150 μm (purple), 100 μm (blue), and 50 μm (light blue) of the ring. Here, the area of averaged cell parameters is independent of ring width (Colour figure online)

common period of water-level and cell data (1961–1986), and so more robust statistical tests were not possible.

In addition to our mean chronology, we investigated how cell parameters varied between trees. First, we calculated the average pairwise correlation between all series (\bar{r}). We then explored the relationship of cell parameters with water-level duration for each tree individually. This allowed us to probe the response of individual trees to changes in water levels. As with the mean cell chronology, we first-differenced each series to remove any long-term trends that would influence the relationship strength. We then calculated Pearson's r between series from different trees and identified significant correlations with a two-tailed test using a 95% confidence interval.

Results

Relationships of tree-ring growth with climate and river discharge

The inter-series correlation of all seven raw ring-width series was 0.61 for years 1940–2020, confirming trees agreed in their patterns of annual growth. Although the resulting chronology extends from 1897 to 2020, it is not robust before 1940. Prior to this year, sample replication is low and the sub-sample signal strength falls below 0.9 (Bunn 2008; Buras 2017). Four of the seven trees had center rings dating between 1941 and 1944, and the youngest tree had a center ring dating to 1952. From 1950 on, tree growth tended to gradually increase before declining from 2003 to present (Fig. 5).

Correlations calculated in SEASCORR show a significant negative relationship ($r = -0.4, p < 0.01$) between tree-ring width and monthly discharge (primary variable) in July, and partial correlations show a significant positive relationship ($r = 0.5, p < 0.01$) with mean temperature (secondary variable) in June, when the intercorrelation of temperature and discharge has been adjusted for (Supplementary Figure 3).

This relationship between growth and July discharge appears to be linear and is significant at this site (Supplemental Figure 4). When precipitation replaces discharge as the primary variable, there is also a significant negative relationship ($r = -0.4, p < 0.01$), but in the month of June. This is expected given that June temperatures should be strongly negatively correlated with June precipitation. These relationships were similar whether or not we included the dammed period (1980–1993) in the analysis, but the correlation strength was weaker when excluding the dammed period (1939–1980).

Macroscopic characteristics of white bands in *Salix*

Rings with terminal white bands could be easily distinguished from years with normal growth (Fig. 1). From 1950 to 1980, terminal white bands occurred in at least one tree every year, peaking in years 1951–1953 and 1959–60. Following these years, the frequency of terminal white bands declined toward the present and almost no white bands were identified after the mid-1980s. There were also important differences between the number of white bands identified per tree (Table 1). For example, tree BSH04 had 23 white

Table 1 List of sampled *Salix alba* trees

Tree	Pith year	Years with early IADFs (1950–2020)	Years with late IADFs (1950–2020)	Years with QWA data
BSH01	1941	5	11	1965–1981
BSH02	1925	0	17	1947–1983
BSH03	1942	3	21	1949–1986
BSH04	1945	17	23	1960–1980
BSH05	1942	7	17	1965–1981
BSH06	1897	4	8	1956–1983
BSH07	1951	0	1	1964–1983

For each tree the pith year (earliest ring), number of years with visually identified early and late IADFs, and the span of time with QWA data is shown

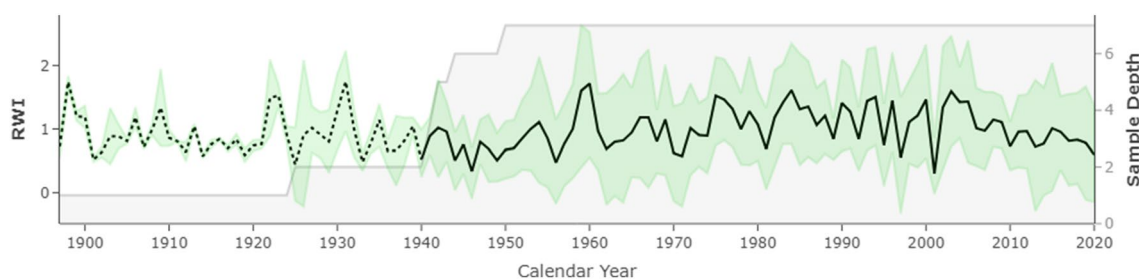


Fig. 5 Detrended tree-ring-width chronology, 1897–2020. Black line is average ring width increment, and dotted portion indicates where sub-sample signal strength falls below 0.9. Tree-ring width detrended using dplR (Bunn 2008). Tree-ring width detrended using dplR (Bunn 2008). Green ribbon is the 95% confidence interval

(i.e., all values within 2 standard deviations of the mean value of the chronology in that year). Gray polygon indicates sample depth in a particular year. The R package 'ggplot2' was used for graphical display (Wickham 2009) (Colour figure online)

bands between 1950 and 2020, but BSH07 only showed 1. It is worth noting that 2001 was an anomalous ‘white ring’ that appeared in every tree. Unlike the white bands described by Yanosky, the entirety of the 2001 ring appeared white. Past research has linked these features to extreme, early-season defoliation events, possibly as a result of an insect outbreak (Hogg et al. 2002; Prendin et al. 2020). This feature, though interesting, displayed no obvious intra-annual variation and so was not categorized as a ring with white bands.

White bands in our samples occur more frequently when trees are young, peaking when trees are between 20 and 30 years old (Fig. 6a). White bands are less common after 35 years of age, occurring in only 1–2 trees per year. This suggests a nonlinear relationship between tree age and white-band frequency, but the matter is complicated by the age distribution of our trees. Five out of our seven trees differ in age by ≤ 10 years. In addition, the oldest tree (BSH06) does display terminal white bands up to 60+ years of age unlike the younger trees. Without collecting more trees of various ages, it is difficult to know if the lack of terminal white bands in recent decades is a function of tree age or environment.

There was only weak evidence that white-band width was related to ring width (Fig. 6b). Only trees BSH02 and BSH03 had significant positive relationships between white-band width and ring width ($r_2=0.52, p_2=0.01; r_3=0.41, p_3=0.05$). All remaining trees except BSH07 had positive but insignificant relationships between white-band width and ring width ($r_1=0.32, p_1=0.33; r_4=0.07, p_4=0.77; r_5=0.10, p_5=0.72; r_6=0.08, p_6=0.65$). BSH07 had only one terminal white band so no relationship could be investigated. This relationship is important because it helps us identify which cell averaging method could best identify white bands. If

white-band width is a function of ring width, then the sectoring approach is preferred because it accounts for the width of the ring in our measurements of white bands. Alternatively, if terminal white bands are independent of ring size, white bands are best characterized by a fixed width and knowing their absolute position in the ring is adequate.

Anatomical characteristics of white bands in *Salix*

Normalizing each cell’s CWT/LA by the average CWT/LA for the non-white portion of the ring did not vastly improve our ability to quantify white bands (Table 2). Normalized p values were much smaller (10^1 – 10^{11} orders of magnitude) than unnormalized p values. In addition, normalizing LA and CWT slightly improved the point-biserial correlation strength ($r_b > 0.04$ – 0.33 in normalized samples) for every ring-division method and for each cell measurement type. However, in all but one case, both normalized and unnormalized cell measurements were able to significantly differentiate between rings with and without terminal white bands ($p < 0.01$). If unnormalized cells can already significantly differentiate between terminal white bands and normal rings, there is little reason to pursue normalization. Given this result, we elected to use unnormalized cell measurements for the remainder of the analysis.

CWT averaged from fiber cells within the terminal 100 μm of the tree ring had the highest average correlation with presence of terminal white bands between all trees ($r_b = -0.51$; Fig. 7). CWT averaged from cells within 50 and 150 μm of the ring boundary had similar but slightly lower average correlations between all trees ($r_b = -0.47$, $r_b = -0.49$). CWT averaged from cells within the last 5%

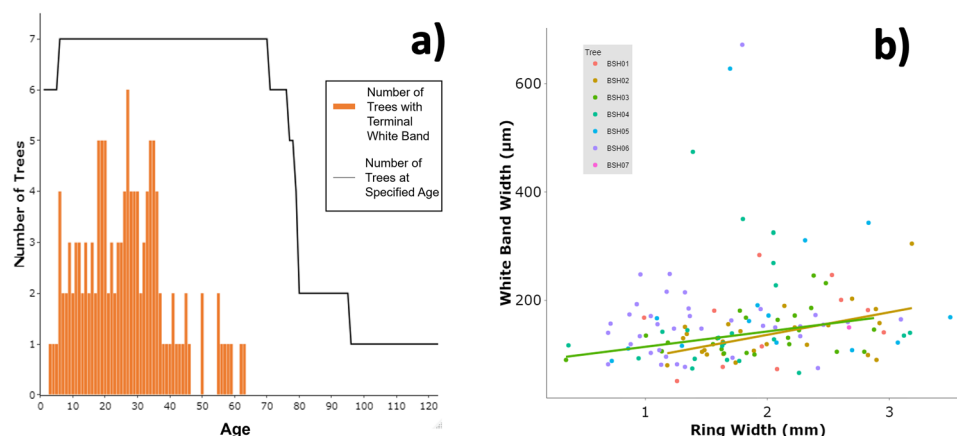


Fig. 6 White band characteristics as they relate to tree age and ring width. **a** Terminal white band frequency as a function of tree age. Orange vertical bars indicate the number of trees that displayed a terminal white band at a particular age. Black line indicates the total number of trees of a certain age. **b** Scatter plot depicting relationship

between ring width and white-band width. Lines of best fit drawn for trees with significant correlations (BSH02: $r_2=0.52, p_2=0.01$; BSH03: $r_3=0.41, p_3=0.05$). When all trees are considered collectively the Pearson correlation between variables is not significant ($r_{\text{all}}=0.13, p_{\text{all}}=0.15$)

Table 2 Comparison of Welch's *t* test values for unnormalized and normalized CWT and LA

Averaging method	CWT		LA	
	Unnormalized	Normalized	Unnormalized	Normalized
87.50%	$t = 5.3$ $df = 150$ $p = 3.7 \times 10^{-7}$	$t = 9.4$ $df = 115.4$ $p = 5.3 \times 10^{-16}$	$t = -1.9$ $df = 174.7$ $p = 0.056$	$t = -7.7$ $df = 123.9$ $p = 3.5 \times 10^{-12}$
90%	$t = 6.3$ $df = 146.4$ $p = 3.5 \times 10^{-9}$	$t = 10.3$ $df = 115.8$ $p < 2.2 \times 10^{-16}$	$t = -3.0$ $df = 173.6$ $p = 0.0032$	$t = -8.6$ $df = 133.8$ $p = 1.5 \times 10^{-14}$
95%	$t = 7.2$ $df = 146.6$ $p = 3.9 \times 10^{-11}$	$t = 10.4$ $df = 120.1$ $p < 2.2 \times 10^{-16}$	$t = -5.1$ $df = 163.9$ $p = 1.2 \times 10^{-6}$	$t = -9.1$ $df = 148.5$ $p = 6.2 \times 10^{-16}$
50 μm	$t = 7.1$ $df = 143.2$ $p = 6.0 \times 10^{-11}$	$t = 9.9$ $df = 126.7$ $p < 2.2 \times 10^{-16}$	$t = -4.6$ $df = 143.0$ $p = 9.5 \times 10^{-6}$	$t = -5.4$ $df = 136.11$ $p = 2.5 \times 10^{-7}$
100 μm	$t = 7.9$ $df = 144.7$ $p = 8.7 \times 10^{-13}$	$t = 11.4$ $df = 120.1$ $p < 2.2 \times 10^{-16}$	$t = -4.4$ $df = 153.7$ $p = 2.1 \times 10^{-5}$	$t = -7.9$ $df = 131.6$ $p = 1.05 \times 10^{-12}$
150 μm	$t = 7.3$ $df = 143.2$ $p = 1.7 \times 10^{-11}$	$t = 11.3$ $df = 114.2$ $p < 2.2 \times 10^{-16}$	$t = -3.3$ $df = 162.4$ $p = 0.0011$	$t = -8.7$ $df = 123.6$ $p = 1.6 \times 10^{-14}$

For each combination of averaging and normalization method, we provide: the test statistic (t), the degrees of freedom (df), and the significance value (p). Normalization resulted in much smaller p values than unnormalized cell parameters, but only in one case (unnormalized LA averaged over >87.5% of the ring) was there a significant difference at $p < 0.05$. Values of $p < 2.2 \times 10^{-16}$ are limited by machine precision

and 10% of each ring also showed correlations within this range ($r_b = -0.47$, $r_b = -0.43$). When rings were divided into 8 sectors (12.5% of total ring area), the correlation strength further decreased ($r_b = -0.37$).

Correlations between LA and presence of terminal white bands were less than that of CWT for all categories listed above. LA correlations were highest for cells within the last 5% of the ring ($r_b = 0.34$). This was followed by LA for cells within 50 μm of the ring boundary ($r_b = 0.33$), within 100 μm of the ring boundary ($r_b = 0.31$), in the last 10% of the ring ($r_b = 0.25$), within 150 μm of the ring boundary ($r_b = 0.23$), and the last 12.5% of the ring ($r_b = 0.13$). To test if increased LA was merely a side effect of decreased CWT, we compared overall fiber cell size (fCS = LA + cell wall area) in the last 10 % of the ring for years that did and did not contain a terminal white band using Tukey's honest significance test (Miller 1981; Yandell 1997). The only significant differences in fCS observed were between the 10% and 80% sectors and the 80% and 100% sectors in rings with terminal white bands ($p < 0.05$; Supplemental Figure 6). Increased LA seen in terminal white bands appears to be a function of decreased CWT, as there is no difference in fCS in the terminal white band and the majority of the growth ring. The significant difference in fCS in the last 70–80% of the ring is consistent with observations of reduced fiber size (Fig. 1b).

The above results justify developing time series from unnormalized CWT measurements for all cell averaging methods. The tests performed above indicate CWT has more power to identify terminal white bands than LA. This makes sense given increased LA is largely a function of reduced CWT. Additionally, unnormalized CWT is nearly as good at identifying terminal white bands in our samples as normalized CWT. However, there was not a clearly preferred approach for cell averaging. CWT within 100 μm of the ring boundary shows the best power to distinguish terminal white bands, but this is nearly matched by the other methods. For these reasons, we develop time series of unnormalized CWT for each cell averaging method and investigate their possible relationships with hydrology below.

Relationship of mean CWT to hydrology

Mean CWT significantly correlated with July water-level durations using both the sectoring and fixed-width cell averaging methods (Fig. 8). All sectoring approaches (averages over the last >87.5%, >90%, and >95% of the ring) were significantly negatively correlated ($p < 0.1$) to the number of days water levels reached or were above 6 m (>87.5%: $r = -0.49$, $p = 0.02$; >90%: $r = -0.47$, $p = 0.03$; >95%: $r = -0.39$, $p = 0.09$). In addition, both the >87.5% and >90%

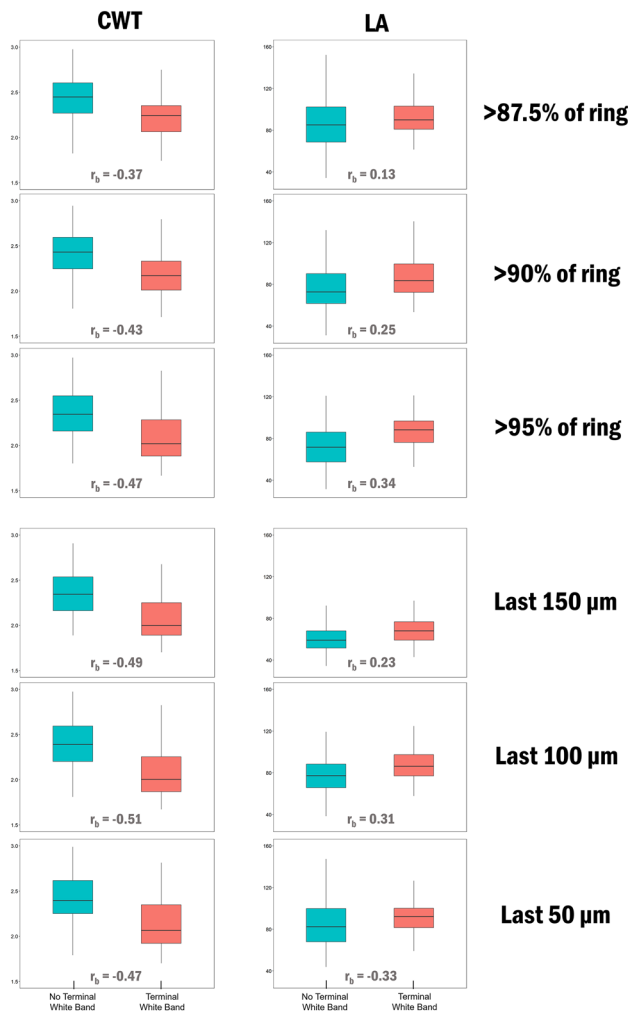


Fig. 7 Comparison of CWT and LA measurements for years without ($n=185$; blue boxplots) and with ($n=92$; red boxplots) terminal white bands, 1947–1986. CWT (first column) is measured in μm and LA (second column) is in units of μm^2 . Each row indicates the cell averaging method used to capture white bands at the end of the growth ring. The years we identified with terminal white bands tend to have lower fiber CWT and higher fiber LA, with generally more variation in the latter. The difference between rings with and without terminal white bands is highly significant ($p < 0.01$, 2-sample t test) for all combinations of cell parameters and averaging method except for LA averaged over $>87.5\%$ of the ring ($p = 0.079$). For comparison of rings with and without terminal white bands by tree, see Supplemental Figure 5 (Colour figure online)

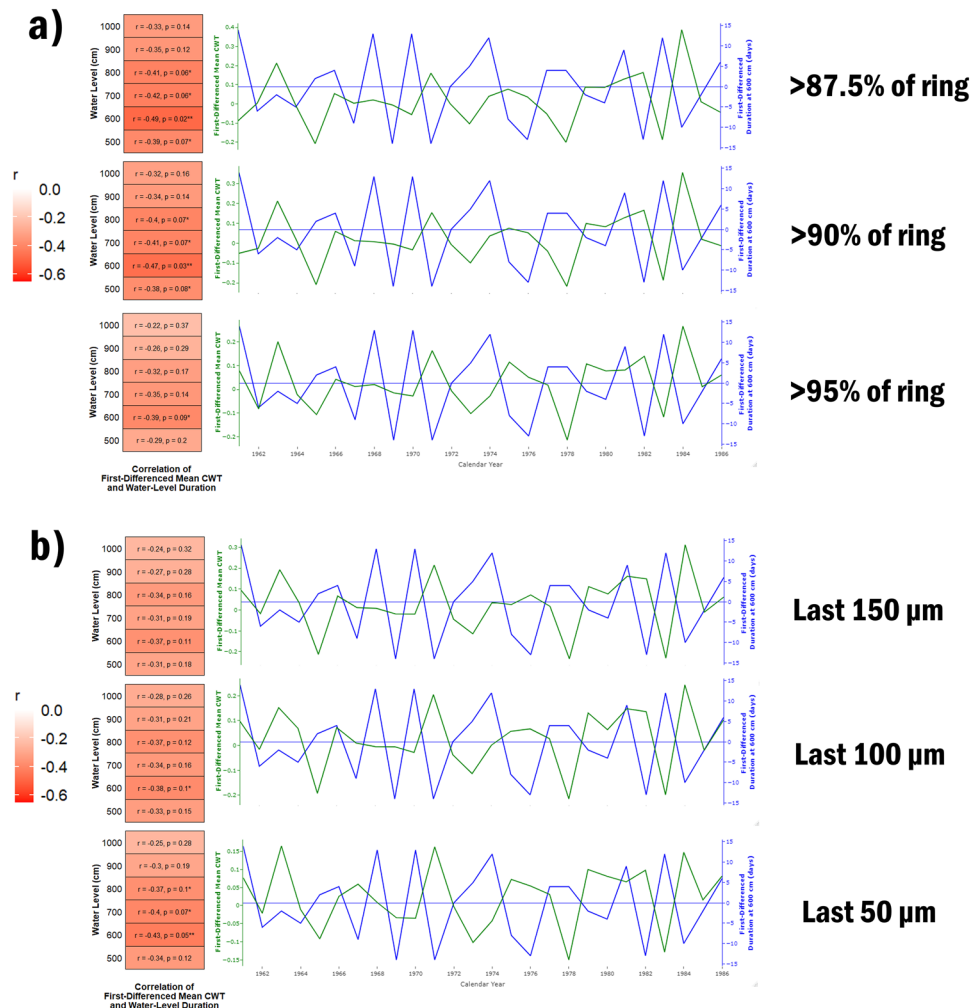
approaches showed significant negative correlations for the number of days water levels spent at or above 5 m ($>87.5\%$: $r = -0.39$, $p = 0.07$; $>90\%$: $r = -0.38$, $p = 0.08$), 7 m ($>87.5\%$: $r = -0.42$, $p = 0.02$; $>90\%$: $r = -0.41$, $p = 0.07$), and 8 m ($>87.5\%$: $r = -0.41$, $p = 0.06$; $>90\%$: $r = -0.40$, $p = 0.07$).

For the fixed-width approach, only CWT time series derived from the last 50 μm and the last 100 μm of each ring showed a significant relationship ($p < 0.1$) to water-level duration. Time series from the last 50 μm were significantly negatively correlated with the number of days water levels rose to or above 6 m ($r = -0.43$, $p = 0.05$), 7 m ($r = -0.4$, $p = 0.07$), and 8 m ($r = -0.37$, $p = 0.1$). In contrast, CWT from the last 100 μm were only related to the duration of water levels at or above 6 m ($r = -0.38$, $p = 0.1$). CWT from the last 150 μm had a weaker relationship to water levels at or above any duration, including at or above 6 m ($r = -0.37$, $p = 0.11$).

CWT of individual trees, regardless of cell averaging method, often does not correlate strongly with other trees. The average pairwise correlation between series, \bar{r} , ranged from 0.03 to 0.08 for all cell averaging methods. Most individual CWT series are slightly positively correlated but these correlations are largely insignificant ($p > 0.1$). Some groupings of trees did emerge, however. Trees BSH02–BSH03 were significantly positively correlated for all cell averaging methods except averages over the last 50 μm ($0.38 < r < 0.45$, $p < 0.05$). Similarly, trees BSH04–BSH06 were significantly positively correlated for all cell averaging methods except over $>95\%$ of the ring and over the last 50 μm ($0.47 < r < 0.58$, $p < 0.05$). Trees BSH04–BSH07 have a significantly negative relationship when CWT was averaged over $>95\%$ of the ring, the last 50 μm , and the last 100 μm ($-0.49 < r < -0.61$, $p < 0.05$).

Although the mean CWT chronology is significantly related to water-level durations, individual tree response was more variable. Only 4 trees showed any significant relationship to water-level durations, the majority of which were negative. CWT of BSH03 was significantly negatively correlated to water-level durations between 7 and 9 m for every averaging method ($-0.42 < r < -0.75$, $p < 0.1$). The strongest of these relationships occurred over all water-level durations for CWT averaged over $>87.5\%$ of the ring ($-0.6 < r < -0.75$, $p < 0.01$; Fig. 9). BSH07 showed significant correlations to water-level durations at or above 5 m for all averaging methods except CWT averaged over $>95\%$ and the last 50 μm of the ring ($-0.47 < r < -0.49$, $p < 0.1$). In contrast, we only found significant negative relationships for BSH05 CWT when averaging over $>95\%$ and the last 50 μm of the ring ($-0.5 < r < -0.56$, $p < 0.1$). Only one significant positive relationship between CWT and water-level durations occurred. CWT of tree BSH04 positively correlated with water-level durations at or above 5 m, but only when averaging over $>87.5\%$ of the ring (Fig. 9). Otherwise the relationship of individual series to water-level durations was largely weak ($r < 0.1$) and insignificant ($p > 0.1$).

Fig. 8 Relationship between mean CWT and the consecutive number of days July water levels were at or above a particular value (1961–1986). Each row indicates the cell averaging method used to capture white bands at the end of the growth ring and generate the mean CWT chronology. The colored columns to the left of the figure show the Pearson correlation strength (r) and significance (p) between the mean CWT chronology and water-level duration at or above each of the specified water levels. Red cells indicate negative correlations and the intensity of the color indicates the correlation strength. The number of asterisks (*) refers to the significance level ($*0.05 < p < 0.1$, $**0.01 < p < 0.05$). The time series to the right of each colored plot is the time series of the specified cell parameter and the number of days water levels exceeded 6 m (Colour figure online)



Discussion

Wood fiber CWT is better for identifying rings with terminal white bands than wood fiber LA. Terminal white bands clearly have both lower CWT and larger LA than cells typically found at the end of the growing season. Although both CWT and LA differed between banded and non-banded rings, the differences were more pronounced with CWT. LA measurements tended to have larger variance within and among trees and this likely reduced its ability to quantify white bands. Differences between CWT and LA persisted regardless of the methodology used to average cells within a band. These results are consistent with finding no difference between total cell area in terminal white bands and the rest of the ring. This supports the idea increased LA is a side effect of decreased CWT, a result we also observe in conifer latewood (Björklund et al. 2017). Our results are also consistent with investigations into fiber characteristics of white rings caused by defoliation. In those studies, average fiber wall thickness could best discriminate between normal years and years where defoliation occurred (Sutton and

Tardif 2005). Therefore, we argue fiber CWT is the preferable measurement for capturing white-band variation in willow rings.

Our results also suggest fiber CWT alone is adequate to quantify terminal white bands. We hypothesized that normalizing CWT (dividing CWT of each cell by the average CWT for the non-white portion of the ring) would improve our ability to distinguish years with and without terminal white bands. Although normalization improved the correlation strength between cell measurements and white-band presence, it did not significantly enhance our ability to detect terminal white bands using fiber CWT. Normalization thus proved unnecessary for quantifying white bands in our samples. This technique may prove more useful in other species, but for parsimony we find it best to use the unnormalized cell measurements.

Unlike normalization, the method used to average CWT measurements matters. For this work, we chose to average CWT over a fixed distance from the ring boundary (the fixed-width approach) and over a certain percentage of the ring (the sectoring approach). The fixed-width approach

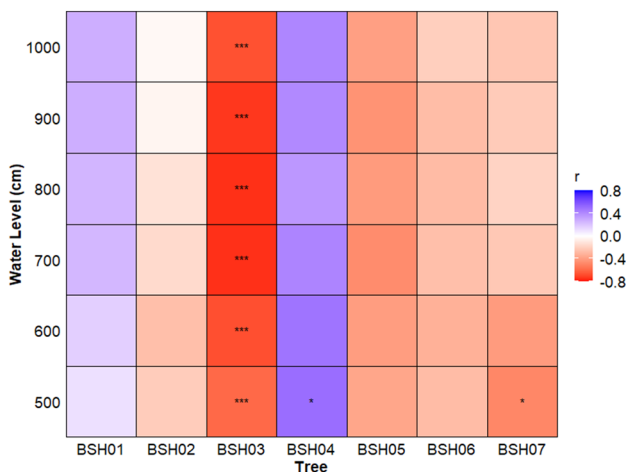


Fig. 9 Example of individual tree correlations between CWT averaged over $> 87.5\%$ of the ring and number of days at or above a particular water level (1961–1986). The x -axis indicates the tree and the y -axis is a particular water level (in centimeters) for the month of July. The color in each cell indicates the correlation between each tree's CWT time series and the consecutive number of days at or above that particular water level. Blue cells indicate positive correlations, red cells indicate negative correlations, and the intensity of the color indicates the correlation strength. The number of asterisks (*) refers to the significance level ($^{*}0.05 <= p <= 0.1$, $^{**}0.01 <= p <= 0.05$, $^{***}0 < p < 0.01$) (Colour figure online)

performed marginally better than the sectoring approach in terms of differentiating rings with and without terminal white bands. However, the mean CWT chronologies derived from the sectoring approach were generally more significantly correlated to durations at or above particular water levels. This was surprising, given that (1) we did not see a strong relationship between ring width and white-band width, and (2) the fixed-width approach was slightly better for identifying white bands. If white-band width correlated only weakly to ring width, we would expect the fixed-width approach to outperform sectoring. Still, using relative cell position is appealing because it better accounts for variations in ring width and can help us better select cells in each year that were produced at the same time (Gebregeorgis et al. 2021).

The evidence does not support our hypothesis that July flooding is related to terminal white band formation in *Salix*. We did not find significant correlations between mean CWT chronologies and the number of days water levels exceeded 10 m, our highest threshold. July water levels would need to reach 12–15 m for flooding to overtop the island, and so it is unlikely that white bands are a flood response. Although both July flood durations and white band frequencies have similar long-term trends, we see that terminal white bands can occur without larger and longer-duration July floods. These similar long-term trends may be an age effect, but we cannot definitively say this without a larger sample size and

trees of various ages. Additionally, the large variability in CWT we see between trees suggests there is an individual response in white band formation.

Our results, however, do suggest that hydrology factors into terminal white band formation. CWT mean chronologies from *Salix* trees in the Yenisei consistently respond to the number of days water levels reached or exceeded 6 m. These chronologies show the negative relationship we would expect if increased moisture causes white-band formation: CWT decreases as the number of days water levels met or exceeded 6 m increases. Water elevations between 6 m above the baseline water level may not be submerging tree stems but may be high enough to reach tree roots. *Salix alba* root systems are generally shallow, with roots of mature trees reaching 0.5–1 m in depth (Bock 1993). The distribution of *Salix* roots within the soil, however, is dependent on the elevation and rooting depth of any particular tree and river discharge dynamics (Pasquale et al. 2012). *Salix* roots visible on some of the island's exposed bluffs appeared to reach at least 1.5–2 m, but the rooting depths of our older sampled trees are unknown. The relationships we see may indicate July water levels are important for saturating the soil and root zone with moisture. The majority of water used by *Salix alba* is from the top 10 cm of the soil, but root water uptake switches to deeper layers later in the growing season (Landgraf et al. 2022).

Additional moisture while soils are saturated could be producing anoxic conditions, affecting normal root function, reducing growth, and causing formation of terminal white bands. This is consistent with our SEASCORR results, which suggest cold and wet conditions in mid- to late-summer decreased growth. While this response appears unusual for an obligate riparian species (e.g., Meko et al. 2015, 2020), it could be due to peak flows in June saturating the soil. Interestingly, the almost complete absence of terminal white bands after the mid-1980s roughly coincides with a complete lack of water levels of > 7 m in July (Fig. 3). In the Yenisei River Basin, reservoir operations began in 1981, reducing summer flows in the northern part of the basin (Yang et al. 2004; Stuefer et al. 2011). Given that the CWT chronology responds strongly to July water levels, it seems possible that this hydrological shift is influencing tree growth.

Although we cannot completely rule out Yanosky's (1984) suggestion that terminal white bands are related to trees benefitting from excess moisture at the end of the growing season, this seems unlikely at this site. For one, cells are optimized to function under normal conditions, so any deviations from that design would imply a stress imposed on the tree, not a benefit (De Micco et al. 2016a, b). Additionally, fiber cell size in terminal white bands is not significantly different from cell size in the majority of the growth ring. The increased fiber LA we see in terminal white bands

is likely just a consequence of reduced fiber CWT and is not related to an increase in fiber cell area that would support Yanosky's claim of increased growth rates. Still, fCS in the last 70–80% of the ring is noticeably different than fCS in the first and last 10% of rings with terminal white bands. These bands of small fibers preceding terminal white bands might be a record of the actual disturbance event, with the tree's recovery and growth post-disturbance manifesting as terminal white bands.

In this way, terminal white bands in *Salix alba* could be related to the physiological changes that occur following annual June flooding. During flood events, the inability of *Salix* roots to absorb nitrogen induces stomatal closure and reduces carbon assimilation and growth (Li et al. 2004, 2005; Fan et al. 2018, 2020). Specific leaf area and nitrogen content in leaves increases during floods, causing flooded willows to grow faster than non-flooded willows post-flood (Rodríguez et al. 2018; Mozo et al. 2021). How much growth occurs depends on post-flood conditions, with droughts following floods most strongly limiting growth (Doffo et al. 2017). This could help explain why hydrological conditions in July are related to terminal white bands in some trees. White bands may not be a flooding response per se, but an artifact of physiological changes caused by June peak flows. It would be useful to compare fiber lumen area and cell wall thickness pre-and post-flood in *Salix* flooded under experimental conditions to better understand if the changes we see here are a direct or indirect response to large flood events. If this were true, it would have important implications for studies examining flood response in tree rings, especially if flooded and non-flooded trees achieve the same overall ring width despite important differences in the timing of wood formation.

There are various caveats to the relationship we identify here, the first of which is the low agreement between trees. CWT did not correlate strongly between trees, which reduces the power of a mean chronology to detect relationships at a site level. Correlations between cell chronologies were mostly positive but extremely weak, and this variation may add considerable noise to any site-level signal. Anatomical features of individual trees may vary in response to differences in microclimate, microtopography, or individual tree sensitivities to external factors but more research is needed to understand how much variability there is. Cell wall thickness of individual trees also responds differently to water levels. While 2–3 trees did respond to increased duration with significantly decreased CWT, other trees showed much weaker correlations, or, in the case of BSH01 and BSH04, positive correlations. Again, differences in rooting depth may explain why not all trees showed a similar pattern.

Given that some trees (e.g., BSH04/BSH05) display many white bands yet show at-best weak correlations to water-level duration, we cannot rule out other potential causes of

white bands. Although Yanosky's work is the only we have found dealing with terminal white bands, multiple studies have identified white rings across genera (e.g., Hogg et al. 2002; Sutton and Tardif 2005; Pederson et al. 2014). In each of these cases, researchers attribute white-ring formation to defoliation caused by insects or a late frost event. The white rings identified in these studies have characteristics that distinguish them from terminal white bands in *Salix*. In experimental defoliation experiments performed by Hogg et al. (2002), white rings only formed when defoliation occurred early in the growing season. Tree defoliation in July and August reduced ring width but did not cause formation of white bands in any part of the growth ring. Additionally, average fiber diameter was significantly smaller in white rings (Jones et al. 2004; Sutton and Tardif 2005). We found no difference in fiber area between terminal white bands and the rest of the ring, indicating fiber size did not significantly decrease in terminal white bands. Similarly, we saw no decrease in ring width following years with white bands that would indicate this was the result of defoliation as described above. For these reasons, a late-summer defoliation event seems an unlikely cause for these terminal white bands.

We suggest terminal white bands in *Salix* are related to hydrology but recognize the need for more research to further substantiate this claim. Although the results suggest CWT in *Salix* is related to duration of water levels > 6 m, our sample size is limited to only 7 trees. Future research can identify how much inter-tree variability plays a role in terminal white-band formation in a given year by using a larger sample size of trees. Although QWA is a time-consuming process, it would also benefit to build longer chronologies of CWT from both our 7 trees and additional samples. Finally, identifying the topographical setting of each tree could shed important light on the differences between trees we see here. Although microsite topography can influence both the level and length of time an individual tree is affected by higher water levels, we expect topography to play only a limited role at our site because we observed little elevational difference between trees (~ 1 m). Still, future work should take care to measure elevations of each sampled tree to rule out any influence of topography on the expression of terminal white bands.

Conclusion

This exploratory analysis not only represents the first time terminal white bands have been quantified using QWA, but is one of only a handful of studies to build time series from measurements of wood fibers in diffuse-porous species. We find that fiber cell wall thickness (CWT) is largely responsible for the appearance of terminal white bands in *Salix* rings

and is a useful parameter for measuring these IADFs. Terminal white bands correlate most strongly with the number of days water levels exceed 6 m at our site, suggesting higher July water levels play a role in their formation. However, we require more research to identify the importance of other factors to terminal white band development. Since factors that influence fiber cells may be tree specific, we recommend future work measure the relative elevation of individual trees above the river's surface and any important microtopography. It would also be informative to compare information from wood fibers to that obtained from vessels, which were not investigated in this study. These two sources could be complimentary, allowing us to better understand what role July flows play in ring-width formation, and providing a better way to interpret how changes in seasonal flows during the growing season affect willow growth.

Author Contribution Statement RT prepared and analyzed data used and drafted the manuscript. IP collected the original samples, helped improve the methodology, provided helpful revisions, and acquired funding. DM helped improve the methodology, provided helpful revisions and acquired funding. GA performed imaging of thin sections and provided critical feedback on the manuscript draft. LA conceived the original idea on anatomical markers of high floods in riparian *Salix* trees, helped with sample collection, and provided critical feedback on the draft manuscript.

Supplementary Information The online version contains supplementary material available at <https://doi.org/10.1007/s00468-023-02386-5>.

Acknowledgements We would like to thank the following people for their contributions to this paper: Angel Simmons for the many hours spent editing cells in ROXAS. Kiyomi Morino and Julie Edwards both contributed their expertise in the form of hands-on training in QWA and ROXAS, respectively. Alexander Shikomanov for providing hydrologic and GIS data. Jia Hu for reading through the initial manuscript and providing critical feedback. David Frank for providing feedback and helpful suggestions.

Funding This study is part of the Tree-Ring Integrated System for Hydrology (TRISH Project) that is supported by funding from U.S. NSF Polar Office program #1917503.

Data availability The datasets generated during and/or analyzed during the current study are available from the corresponding author on reasonable request.

Declarations

Conflict of interest The authors declare no conflicts of interest.

Open Access This article is licensed under a Creative Commons Attribution 4.0 International License, which permits use, sharing, adaptation, distribution and reproduction in any medium or format, as long as you give appropriate credit to the original author(s) and the source, provide a link to the Creative Commons licence, and indicate if changes were made. The images or other third party material in this article are

included in the article's Creative Commons licence, unless indicated otherwise in a credit line to the material. If material is not included in the article's Creative Commons licence and your intended use is not permitted by statutory regulation or exceeds the permitted use, you will need to obtain permission directly from the copyright holder. To view a copy of this licence, visit <http://creativecommons.org/licenses/by/4.0/>.

References

Agafonov LI, Meko DM, Panyushkina IP (2016) Reconstruction of Ob River, Russia, discharge from ring widths of floodplain trees. *J Hydrol* 543:198–207. <https://doi.org/10.1016/j.jhydrol.2016.09.031>

Anadon-Rosell A, Scharnweber T, von Arx G et al (2022) Growth and wood trait relationships of *Alnus glutinosa* in peatland forest stands with contrasting water regimes. *Front Plant Sci* 12:2988. <https://doi.org/10.3389/fpls.2021.788106>

Arbellay E, Corona C, Stoffel M et al (2012) Defining an adequate sample of earlywood vessels for retrospective injury detection in diffuse-porous species. *PLoS One* 7:e38824. <https://doi.org/10.1371/journal.pone.0038824>

Ballesteros JA, Stoffel M, Bollschweiler M et al (2010) Flash-flood impacts cause changes in wood anatomy of *Alnus glutinosa*, *Fraxinus angustifolia* and *Quercus pyrenaica*. *Tree Physiol* 30:773–781. <https://doi.org/10.1093/TREEPHYSP/TPQ031>

Ballesteros-Cánovas JA, Stoffel M, St George S, Hirschboeck K (2015) A review of flood records from tree rings. *Prog Phys Geogr* 39:794–816. <https://doi.org/10.1177/0309133315608758>

Beck HE, Zimmermann NE, McVicar TR et al (2018) Present and future köppen-geiger climate classification maps at 1-km resolution. *Sci Data* 5:1–12. <https://doi.org/10.1038/sdata.2018.214>

Bedrick EJ (2005) Biserial Correlation. *Encycl Biostat*. <https://doi.org/10.1002/0470011815.B2A10007>

Björklund J, Seftigen K, Schweingruber F et al (2017) Cell size and wall dimensions drive distinct variability of earlywood and late-wood density in Northern Hemisphere conifers. *New Phytol*. <https://doi.org/10.1111/nph.14639>

Bock EN (1993) Geographical and hydrological aspects of willow regeneration in Ob-Irtysh floodplain. *Geogr Nat Resour (russian Journal)* 1:94–100

Bring A, Shiklomanov A, Lammers RB (2017) Pan-Arctic river discharge: Prioritizing monitoring of future climate change hot spots. *Earth's Futur* 5:72–92. <https://doi.org/10.1002/ef2.175>

Brown MB, Forsythe AB (1974) Robust Tests for the Equality of Variances. *J Am Stat Assoc* 69:364. <https://doi.org/10.2307/2285659>

Bunn AG (2008) A dendrochronology program library in R (dplR). *Dendrochronologia* 26:115–124. <https://doi.org/10.1016/J.DENDRO.2008.01.002>

Buras A (2017) A comment on the expressed population signal. *Dendrochronologia* 44:130–132. <https://doi.org/10.1016/J.DENDRO.2017.03.005>

Carlquist SJ (2001) Comparative Wood Anatomy: Systematic, Ecological, and Evolutionary Aspects of Dicotyledon Wood. 448

Carmack EC, Yamamoto-Kawai M, Haine TWN et al (2016) Freshwater and its role in the Arctic Marine System: Sources, disposition, storage, export, and physical and biogeochemical consequences in the Arctic and global oceans. *J Geophys Res G Biogeosciences* 121:675–717. <https://doi.org/10.1002/2015JG003140>

Coumou D, Di Capua G, Vavrus S, et al (2018) The influence of Arctic amplification on mid-latitude summer circulation. *Nat Commun* 9

Dawdy D, Matalas N (1964) Statistical and Probability Analysis of Hydrologic Data, Part III: Analysis of Variance. McGraw-Hill, Covariance and Time Series

De Micco V, Battipaglia G, Balzano A et al (2016a) Are wood fibres as sensitive to environmental conditions as vessels in tree rings with intra-annual density fluctuations (IADFs) in Mediterranean species? *Trees Str Funct* 30:971–983. <https://doi.org/10.1007/S00468-015-1338-5/FIGURES/5>

De Micco V, Campelo F, De Luis M et al (2016b) Intra-annual density fluctuations in tree rings: How, when, where, and why? *IAWA J* 37:232–259. <https://doi.org/10.1163/22941932-20160132>

Doffo GN, Monteoliva SE, Rodríguez ME, Luquez VMC (2017) Physiological responses to alternative flooding and drought stress episodes in two willow (*Salix* spp.) clones. *Can J For Res* 47:174–182. <https://doi.org/10.1139/CJFR-2016-0202/SUPPLFILE/CJFR-2016-0202SUPPL.PDF>

Edwards J, Anchukaitis KJ, Zambri B et al (2020) Intra-Annual Climate Anomalies in Northwestern North America Following the 1783–1784 CE Laki Eruption. *J Geophys Res Atmos* 126:1–22. <https://doi.org/10.1029/2020JD033544>

Fan R, Morozumi T, Maximov TC, Sugimoto A (2018) Effect of floods on the $\delta^{13}\text{C}$ values in plant leaves: A study of willows in Northeastern Siberia. *PeerJ*. <https://doi.org/10.7717/PEERJ.5374/SUPP-10>

Fan R, Tanekura K, Morozumi T et al (2020) Adaptation of willows in river lowlands to flooding under arctic amplification: evidence from nitrogen content and stable isotope dynamics. *Wetlands* 40:2413–2424. <https://doi.org/10.1007/S13157-020-01353-X/FIGURES/13>

Feng D, Gleason CJ, Lin P et al (2021) Recent changes to Arctic river discharge. *Nat Commun* 12(12):1–9. <https://doi.org/10.1038/s41467-021-27228-1>

Gans DJ (1981) Use of a preliminary test in comparing two sample means. *Commun Stat Simul Comput* 10:163–174

Gastwirth JL, Gel YR, Miao W (2009) The impact of levene's test of equality of variances on statistical theory and practice. *Statist Sci* 24:343–360. <https://doi.org/10.1214/09-STS301>

Gebregeorgis EG, Boniecka J, Piątkowski M, et al (2021) SabaTracheid 1.0: a novel program for quantitative analysis of conifer wood anatomy — a demonstration on African Juniper from the Blue Nile Basin. *Front Plant Sci* 12:21. <https://doi.org/10.3389/fpls.2021.595258>

Hacke UG, Sperry JS, Pockman WT et al (2000) (2001) Trends in wood density and structure are linked to prevention of xylem implosion by negative pressure. *Oecologia* 126(126):457–461. <https://doi.org/10.1007/S004420100628>

He F, Clark PU (2022) Freshwater forcing of the Atlantic Meridional Overturning Circulation revisited. *Nat Clim Chang* 12:449–454. <https://doi.org/10.1038/s41558-022-01328>

Hogg EH, Hart M, Lieffers VJ (2002) White tree rings formed in trembling aspen saplings following experimental defoliation. *Canadian J For Res*. <https://doi.org/10.1139/X02-114>

Hu J, Emile-Geay J, Partin J (2017) Correlation-based interpretations of paleoclimate data – where statistics meet past climates. *Earth Planet Sci Lett* 459:362–371. <https://doi.org/10.1016/J.EPSL.2016.11.048>

IPCC (2021) Climate change 2021: The physical science basis. Contribution of working group I to the Sixth assessment report of the intergovernmental panel on climate change

Jacobs P, Viechtbauer W (2016) Estimation of the biserial correlation and its sampling variance for use in meta-analysis. *Res Synth Methods*. <https://doi.org/10.1002/jrsm.1218>

Janssen TAJ, Hölttä T, Fleischer K et al (2020) Wood allocation trade-offs between fiber wall, fiber lumen, and axial parenchyma drive drought resistance in neotropical trees. *Plant Cell Environ* 43:965–980. <https://doi.org/10.1111/PCE.13687>

Jones B, Tardif J, Westwood R (2004) Weekly xylem production in trembling aspen (*Populus tremuloides*) in response to artificial defoliation. *Can J Bot* 82:590–597. <https://doi.org/10.1139/B04-032>

Jones EP, Anderson LG, Jutterström S et al (2008) Pacific freshwater, river water and sea ice meltwater across Arctic Ocean basins: Results from the 2005 Beringia Expedition. *J Geophys Res* 113:1–10. <https://doi.org/10.1029/2007jc004124>

Kames S, Tardif JC, Bergeron Y (2016) Continuous earlywood vessels chronologies in floodplain ring-porous species can improve dendrohydrological reconstructions of spring high flows and flood levels. *J Hydrol* 534:377–389. <https://doi.org/10.1016/J.JHYDROL.2016.01.002>

Landgraf J, Tetzlaff D, Dubbert M et al (2022) Xylem water in riparian willow trees (*Salix alba*) reveals shallow sources of root water uptake by *in situ* monitoring of stable water isotopes. *Hydrol Earth Syst Sci* 26:2073–2092. <https://doi.org/10.5194/HESS-26-2073-2022>

Li S, Pezeshki SR, Goodwin S, Shields FD (2004) Physiological responses of black willow (*Salix nigra*) cuttings to a range of soil moisture regimes. *Photosynth* 42:585–590. <https://doi.org/10.1007/S11099-005-0017-Y>

Li S, Martin LT, Pezeshki SR et al (2005) Responses of black willow (*Salix nigra*) cuttings to simulated herbivory and flooding. *AcO* 28:173–180. <https://doi.org/10.1016/J.ACTAO.2005.03.009>

López J, Del Valle JI, Giraldo JA (2014) Flood-promoted vessel formation in *Prioria copaifera* trees in the Darien Gap, Colombia. *Tree Physiol* 34:1079–1089. <https://doi.org/10.1093/TREEPHYS/TPU077>

MacDonald GM, Kremenetski KV, Smith LC, Hidalgo HG (2007) Recent Eurasian river discharge to the Arctic Ocean in the context of longer-term dendrohydrological records. *J Geophys Res Biogeosci*. <https://doi.org/10.1029/2006JG000333>

Meko MD, Therrell MD (2020) A record of flooding on the White River, Arkansas derived from tree-ring anatomical variability and vessel width. *Phys Geogr* 41:83–98. <https://doi.org/10.1080/02723646.2019.1677411>

Meko DM, Touchan R, Anchukaitis KJ (2011) Seascorr: A MATLAB program for identifying the seasonal climate signal in an annual tree-ring time series. *Comput Geosci* 37:1234–1241. <https://doi.org/10.1016/J.CAGEO.2011.01.013>

Meko DM, Woodhouse CA, Morino K (2012) Dendrochronology and links to streamflow. *J Hydrol* 412–413:200–209. <https://doi.org/10.1016/j.jhydrol.2010.11.041>

Meko DM, Friedman JM, Touchan R et al (2015) Alternative standardization approaches to improving streamflow reconstructions with ring-width indices of riparian trees. *Holocene* 25:1093–1101. <https://doi.org/10.1177/0959683615580181>

Meko DM, Panyushkina IP, Agafonov LI, Edwards JA (2020) Impact of high flows of an Arctic river on ring widths of floodplain trees. *Holocene* 30:789–798. <https://doi.org/10.1177/0959683620902217>

Menne MJ, Williams CN, Gleason BE, Rennie JJ, Lawrimore JH (2018) The Global Historical Climatology Network Monthly Temperature Dataset, Version 4. *J. Climate*, in press. <https://doi.org/10.1175/JCLI-D-18-0094.1>

Miller RG (1981) *Simultaneous Statistical Inference*. Springer, New York

Mozo I, Rodríguez ME, Monteoliva S, Luquez VMC (2021) Flood-water Depth causes different physiological responses during post-flooding in willows. *Front Plant Sci*. <https://doi.org/10.3389/fpls.2021.575090>

Nolin AF, Tardif JC, Conciatori F et al (2021) Multi-century tree-ring anatomical evidence reveals increasing frequency and magnitude of spring discharge and floods in eastern boreal Canada.

Glob Planet Change 199:103444. <https://doi.org/10.1016/J.GLOPLACHA.2021.103444>

Panyushkina IP, Meko D, Shiklomanov A et al (2021) Unprecedented acceleration of winter discharge of Upper Yenisei River inferred from tree rings. Environ Res Lett. <https://doi.org/10.1088/1748-9326/ac3e20>

Pasquale N, Perona P, Francis R, Burlando P (2012) Effects of streamflow variability on the vertical root density distribution of willow cutting experiments. Ecol Eng 40:167–172. <https://doi.org/10.1016/J.ECOLENG.2011.12.002>

Pederson N, Dyer JM, McEwan RW et al (2014) The legacy of episodic climatic events in shaping temperate, broadleaf forests. Ecol Monogr 84:599–620

Peters RL, Balanzategui D, Hurley AG et al (2018) RAPTOR: Row and position tracheid organizer in R. Dendrochronologia 47:10–16. <https://doi.org/10.1016/j.dendro.2017.10.003>

Porter C, Morin P, Howat I, et al (2018) ArcticDEM. In: Harvard Dataverse, V1. <https://dataVERSE.harvard.edu/dataset.xhtml?persistentId=doi:10.7910/DVN/OHHUKH>. Accessed 26 Apr 2022

Prendin AL, Carrer M, Karami I Mojtaba, et al (2020) Immediate and carry-over effects of insect outbreaks on vegetation growth in West Greenland assessed from cells to satellite. J Biogeogr. <https://doi.org/10.1111/jbi.13644>

R Core Team (2020) R: A language and environment for statistical computing. R Foundation for Statistical Computing, Vienna, Austria. <https://www.R-project.org/>

Rizopoulos D (2007) ltm: An R Package for Latent Variable Modeling and Item Response Analysis. J Stat Softw 17:1–25. <https://doi.org/10.18637/JSS.V017.I05>

Rodríguez ME, Doffo GN, Cerrillo T, Luquez VMC (2018) Acclimation of cuttings from different willow genotypes to flooding depth level. New For 49:415–427. <https://doi.org/10.1007/s11056-018-9627-7>

Royston P (1995) Remark AS R94: A remark on algorithm AS 181: The W-test for normality. Appl Stat 44:547. <https://doi.org/10.2307/2986146>

Schoch W, Heller-Kellenberger I, Schweingruber F, Kienast F, Schmatz D (2004) Wood anatomy of central European species. <https://www.wsl.ch/land/products/dendro/species.php?code=SAAL>

Screen JA, Simmonds I (2010) The central role of diminishing sea ice in recent Arctic temperature amplification. Nature 464:1334–1337. <https://doi.org/10.1038/nature09051>

Serreze MC, Francis JA (2006) The Arctic on the fast track of change. Weather 61:65–69. <https://doi.org/10.1256/wea.197.05>

Shapiro SS, Wilk MB (1965) An analysis of variance test for normality (Complete Samples). Biometrika 52:591. <https://doi.org/10.2307/2333709>

Shiklomanov AI, Lammers RB (2009) Record Russian river discharge in 2007 and the limits of analysis. Environ Res Lett 4:1–9. <https://doi.org/10.1088/1748-9326/4/4/045015>

Shiklomanov AI, Lammers RB, Lettenmaier DP et al (2013) Hydrological Changes: Historical Analysis, Contemporary Status, and Future Projections. Regional Environmental Changes in Siberia and Their Global Consequences. Springer, Dordrecht, pp 111–154

Smith LC, Stephenson SR (2013) New Trans-Arctic shipping routes navigable by midcentury. PNAS 110:E1191–E1195. <https://doi.org/10.1073/pnas.1214212110>

Stuefer S, Yang D, Shiklomanov A (2011) Effect of streamflow regulation on mean annual discharge variability of the Yenisei River. 346:

Sutton A, Tardif J (2005) Distribution and anatomical characteristics of white rings in *Populus tremuloides*. IAWA J 26:221–238

Tardif JC, Dickson H, Conciatori F et al (2021) Are periodic (intra-annual) tangential bands of vessels in diffuse-porous tree species the equivalent of flood rings in ring-porous species? Reproducibility and cause. Dendrochronologia 70:125889. <https://doi.org/10.1016/J.DENDRO.2021.125889>

Tyree MT, Ewers FW (1991) The hydraulic architecture of trees and other woody plants. New Phytol 119:345–360. <https://doi.org/10.1111/j.1469-8137.1991.tb00035.x>

von Arx G, Carrer M (2014) ROXAS-A new tool to build centuries-long tracheid-lumen chronologies in conifers. Dendrochronologia 32:290–293. <https://doi.org/10.1016/j.dendro.2013.12.001>

von Arx G, Kueffer C, Fonti P (2013) Quantifying plasticity in vessel grouping - Added value from the image analysis tool ROXAS. IAWA J 34:433–445. <https://doi.org/10.1163/22941932-00000035>

Wegner L, Eilmann B, Sass-Klaassen U, Von Arx G (2013) ROXAS – an efficient and accurate tool to detect vessels in diffuse-porous species. IAWA J 34:425–432. <https://doi.org/10.1163/22941932-00000034>

Weijer W, Cheng W, Garuba OA et al (2020) CMIP6 models predict significant 21st Century Decline Of The Atlantic Meridional Overturning Circulation. Geophys Res Lett. <https://doi.org/10.1029/2019GL086075>

Wickham H (2009) ggplot2. ggplot2. <https://doi.org/10.1007/978-0-387-98141-3>

Yamaguchi DK (2011) A simple method for cross-dating increment cores from living trees. Can J For Res 21:414–416. <https://doi.org/10.1139/X91-053>

Yandell BS (1997) Practical data analysis for designed experiments. CRC Press

Yang D, Ye B, L. Kane D, (2004) Streamflow changes over Siberian Yenisei River Basin. J Hydrol 296:59–80. <https://doi.org/10.1016/J.JHYDROL.2004.03.017>

Yanosky TM (1984) Documentation of high summer flows on the Potomac River from the wood anatomy of ash trees. J Am Water Resour Assoc 20:241–250. <https://doi.org/10.1111/j.1752-1688.1984.tb04678.x>

Zanowski H, Jahn A, Holland MM (2021) Arctic ocean freshwater in CMIP6 Ensembles: declining sea ice, increasing ocean storage, and export. J Geophys Res Ocean. <https://doi.org/10.1029/2020JC016930>

Publisher's Note Springer Nature remains neutral with regard to jurisdictional claims in published maps and institutional affiliations.